

1 **Assessment of dicarbonyl contributions to secondary organic aerosols over China**  
2 **using RAMS-CMAQ**

3 Jialin Li <sup>1</sup>, Meigen Zhang <sup>1,2,3,\*</sup>, Guiqian Tang <sup>1</sup>, Yele Sun <sup>1,2,3</sup>, Fangkun Wu <sup>1</sup>,  
4 Yongfu Xu <sup>1,3</sup>

5  
6 <sup>1</sup>State Key Laboratory of Atmospheric Boundary Layer Physics and Atmospheric Chemistry,  
7 Institute of Atmospheric Physics, Chinese Academy of Sciences, Beijing 100029, China

8 <sup>2</sup>Center for Excellence in Regional Atmospheric Environment, Institute of Urban Environment,  
9 Chinese Academy of Sciences, Xiamen 361021, China

10 <sup>3</sup>University of Chinese Academy of Sciences, Beijing 100049, China

11  
12 **Abstract**

13 The concentration of secondary organic aerosol (SOA) is underestimated in current model studies.  
14 Recent research suggests that the reactive uptake of dicarbonyls contributes to the production of  
15 SOA, although few models have included this pathway. Glyoxal, an important representative  
16 component of dicarbonyls in models, is significantly underestimated. We therefore incorporated the  
17 reactive uptake of dicarbonyls into the regional air quality modeling system RAMS-CMAQ (the  
18 Regional Atmospheric Modeling System-Community Multiscale Air Quality) to evaluate the  
19 contribution of dicarbonyls to SOA, and we then assess the impact of the underestimation of glyoxal  
20 on the production of SOA in China during two time periods: June 3 to July 11, 2014 (episode 1) and  
21 October 14 to November 14, 2014 (episode 2). When the reactive uptake process was added, the  
22 modeled mean concentration of SOA in episode 1 increased by 3.65  $\mu\text{g}/\text{m}^3$ , which explained 34.8%  
23 of the unaccounted source of SOA. Whereas the increase in the concentration of SOA in episode 2  
24 was 1.82  $\mu\text{g}/\text{m}^3$  as a result of the lower liquid water content and the lower amount of dicarbonyls  
25 produced from biogenic precursors in the fall. On this basis, when the glyoxal simulation was  
26 improved, the modeled mean dicarbonyl-derived SOA (AAQ) increased by more than a factor of 2  
27 in both episodes relative to case 1. AAQ in episode 1 contributed, on average, 60.6% of the total  
28 concentration of SOA and the increase in this contribution represented 69.1% of the unaccounted  
29 concentration of SOA, whereas the mean AAQ in episode 2 accounted for 64.5% of total  
30 concentration of SOA. Based on the results, the mean AAQ over China was generally higher in the  
31 east than in the west during the two episodes. The highest value (10–15  $\mu\text{g}/\text{m}^3$ ) of episode 1 appeared

32 in the areas around the lower reaches of the Yellow River. Whereas the highest value of 5–10  $\mu\text{g}/\text{m}^3$   
33 in episode 2 was concentrated over regions from south of the lower reaches of the Yellow River to  
34 the south of Guangzhou Province as well as the Sichuan Basin. The contribution of AAQ to the  
35 concentration of SOA in episode 1 varied from 10 to 90% throughout China, with the highest  
36 contributions (70–90%) in the coastal regions and offshore along the East China Sea to the South  
37 China Sea and in the southwestern regions. Whereas the fraction of AAQ to SOA in episode 2 was  
38 in the range of 10–80% over China, with the fraction up to 80% in a small portion of northeastern  
39 China.

40 **Keywords:** secondary organic aerosol, reactive uptake, glyoxal, China, RAMS-CAMQ

41

## 42 **1. Introduction**

43 The fine particle fraction of aerosols ( $\text{PM}_{2.5}$ , i.e., particulate matter with an aerodynamic diameter  
44  $\leq 2.5 \mu\text{m}$ ) not only absorbs and scatters sunlight in the atmosphere, resulting in a reduction in  
45 visibility and effects on the global climate (IPCC, 2007), but also has adverse effects on human  
46 health (Harrison and Yin, 2000;Poschl, 2005). Organic aerosol (OA) is a major component of fine  
47 particulate matter globally (Murphy et al., 2006;Zhang et al., 2007), typically making up 20–90%  
48 of the fine particle fraction (Roberts et al., 2001;Kanakidou et al., 2005;Zhang et al., 2007),  
49 suggesting that it has a significant effect on the characteristics and properties of fine particulate  
50 matter. Organic aerosols are formed from both primary (direct emissions) and secondary sources.  
51 Secondary organic aerosols (SOAs) are formed from precursors of volatile organic compounds  
52 (VOCs), which can be either natural or anthropogenic. However, the underestimation of organic  
53 aerosol has become a major issue in almost all current atmospheric models due to the incomplete  
54 representation of SOA (Heald et al., 2005;Morris et al., 2005;Morris et al., 2006;Goldstein and  
55 Galbally, 2007;Yu et al., 2008;Fu et al., 2009;Farina et al., 2010;Jiang et al., 2012;Zhang and Ying,  
56 2012;Jo et al., 2013;Lin et al., 2016).

57 It has been reported that the concentration of SOA in the models is underestimated by one to two  
58 orders of magnitude (de Gouw et al., 2005;Volkamer et al., 2006). These results have motivated  
59 researchers to investigate why these models are predicting SOA concentrations so poorly.  
60 Traditionally, improvements in models have mainly concentrated on the gas-phase and derived  
61 heterogeneous formation processes, such as the formation of SOA from aromatic compounds under

62 low- and high-NO<sub>x</sub> conditions (Ng et al., 2007), the production of SOA from the oxidation of  
63 isoprene and its subsequent growth through acid catalysis (Kroll et al., 2005, 2006;Surratt et al.,  
64 2007), the use of volatile bias set method to depict the formation of SOA instead of the two-product  
65 model (Lane et al., 2008;Murphy and Pandis, 2009;Han et al., 2016;Lin et al., 2016), and the  
66 formation of SOA through the uptake of isoprene epoxides on the surface of aerosols (Ying et al.,  
67 2015;Hu et al., 2017). The gap has been closed to some degree through the SOA modeling efforts,  
68 but there are still large uncertainties (Tsigaridis et al., 2014).

69 Many studies have suggested that glyoxal and methylglyoxal can form SOAs through chemical  
70 reactions in cloud or fog water (e.g. Warneck, 2003;Ervens et al., 2004;Lim and Ziemann,  
71 2005;Carlton et al., 2006;Loeffler et al., 2006), or by reactive uptake on the surface of cloud droplets  
72 and aqueous aerosols (e.g. Liggio et al., 2005;Corrigan et al., 2008;Galloway et al., 2009;Ervens  
73 and Volkamer, 2010;Lim et al., 2010), which is probably a significant source of SOA (Ervens et al.,  
74 2014;Curry et al., 2018). A few studies (e.g. Carlton et al., 2008;Fu et al., 2009;Carlton et al.,  
75 2010;Lin et al., 2012;Li et al., 2013;Lin et al., 2014;Woo and McNeill, 2015) have incorporated  
76 aqueous SOA formation pathways into atmospheric models. Several of these studies have shown  
77 that chemical reactions only in cloud or fog water make negligible contribution to near-surface SOA  
78 relative to reactive uptake on the surface of cloud droplets and aqueous aerosols, and that the  
79 aqueous SOA formation cannot completely explain the gaps between the observations and  
80 simulations. There are still considerable uncertainties in our knowledge of the formation of SOA.

81 A series of studies (Fu et al., 2008;Myriokefalitakis et al., 2008;Liu et al., 2012;Li et al., 2018)  
82 has shown that there is a substantial underestimation in the modeled vertical column densities  
83 (VCDs) of glyoxal, but few studies have considered the impact of this underestimation on  
84 simulations of SOA concentrations. Xu et al. (2017) and Ervens et al. (2011) showed that the  
85 aqueous SOA formation depends on the liquid water content (LWC), which varies between seasons.  
86 Previous studies, such as those of Fu et al. (2009) and Li et al. (2013), have only considered the  
87 contribution from SOA derived from the reactive uptake of dicarbonyls (pathway M) in the summer  
88 period or over evergreen areas. In this study, we not only incorporated pathway M into the RAMS-  
89 CMAQ (the Regional Atmospheric Modeling System-Community Multiscale Air Quality) modeling  
90 system to evaluate the corresponding contribution of dicarbonyls to SOA, but also improved the  
91 simulation of glyoxal concentrations by investigating the reasons for its underestimation and

92 assessing its impacts on the concentration of SOA during the two episodes in the summer and fall  
93 of China.

94

## 95 **2. Model and data**

### 96 **2.1 Base model description**

97 Li et al. (2017a) used the RAMS-CMAQ modeling system to investigate the effects of  
98 underestimated aromatic VOC emissions and yields of SOAs from different gas precursors on the  
99 concentration of SOAs. Similarly, we used Version 4.7.1 of the CMAQ, which is coupled with the  
100 gas-phase photochemical mechanism SAPRC99 (1999 Statewide Air Pollutant Research Center  
101 (Carter, 2000) and Version 5 of the aerosol module (AERO5) (Byun and Schere, 2006;Foley et al.,  
102 2010). There are three major formation pathways for SOAs in this version. Based on the two-product  
103 approach, the first pathway is the equilibrium partition of semi-volatile products formed from the  
104 oxidation of seven VOC precursors: long-chain alkanes, benzene (BNZ), high-yield aromatics  
105 (mainly toluene, ARO1), low-yield aromatics (mainly xylene, ARO2), isoprene (ISOP),  
106 monoterpene (TRP) and sesquiterpenes (SESQ). The second pathway is the oligomerization of  
107 semi-volatile SOAs formed through the first pathway (Kalberer et al., 2004), namely aging process.  
108 The third pathway is the formation of SOA via the in-cloud oxidation of glyoxal (GLY) and  
109 methylglyoxal (MGLY) (Carlton et al., 2008), both of which represent dicarbonyls in the model.  
110 The details of these formation pathways are given in Carlton et al. (2010).

111 The meteorological fields used to drive CMAQ are obtained from RAMS, which has been  
112 described in detail by Cotton et al. (2003). The National Centers for Environmental Prediction  
113 reanalysis datasets are served as the initial and lateral boundary meteorological conditions input into  
114 RAMS. The boundary conditions used for the RAMS computations include the weekly average sea  
115 surface temperature and the monthly measured snow cover. The final modeled results are output  
116 through the four-dimensional data assimilation mode using nudging analysis.

117 The emission sources are derived from several different inventories. Anthropogenic emissions (Li  
118 et al., 2017b)—including SO<sub>2</sub>, NO<sub>x</sub>, CO, black carbon, non-methane VOCs, organic carbon, NH<sub>3</sub>  
119 and other particulate matter—are obtained from the monthly emissions inventory of 2012. There are  
120 five emission sectors (the power, industrial, residential, transportation and agricultural sectors) in  
121 the inventory with a spatial resolution of 0.25° × 0.25° (see [www.meicmodel.org](http://www.meicmodel.org)). The Model of

122 Emissions of Gases and Aerosols from Nature (MEGAN) (Guenther et al., 2012) provides the  
123 biogenic emissions. The emissions from open biomass burning are derived from the Global Fire  
124 Emissions Database, Version 4 (Randerson et al., 2015), whereas the information of monthly  
125 lightning NO<sub>x</sub> is obtained from the Global Emissions Inventory Activity with a spatial resolution of  
126 1° × 1° (Benkovitz et al., 1996). The emissions of NO<sub>x</sub> from the soil are derived from the Regional  
127 Emission inventory in ASia, Version 2.1, with a spatial resolution of 0.25° × 0.25° (Kurokawa et al.,  
128 2013). The online dust and sea salt emissions are calculated using the empirical model developed  
129 by Han et al. (2004) and the scheme of Gong (2003), respectively. The calculation of the model  
130 boundary conditions is supported by the Model of Ozone and Related Tracers, Version 4 (MOZART-  
131 4) (Emmons et al., 2010).

132 The model domain is divided into 105 × 86 grid cells with the center located at (35° N, 110° E)  
133 (Fig. 1). The map projection is rotated polar-stereographic with a horizontal resolution of 64 km.  
134 The vertical simulation region is unequally spaced from the ground surface to ~23 km. There are 25  
135 layers in the σ<sub>z</sub> coordinate system in RAMS, with nine layers located in the lowest 2 km to resolve  
136 the planetary boundary layer. The vertical dimension of CMAQ is divided into 15 layers, with the  
137 lowest seven layers the same as those in RAMS. We focused on the area outlined by the blue box in  
138 Fig. 1.

139

## 140 **2.2 Adding the reactive uptake process**

141 There is a standard reaction probability formulation for reactive uptake of gases by aerosols and  
142 clouds in Jacob (2000). In this formulation, the first-order rate constant  $k$  for the chemical loss of a  
143 gas-phase species to the aerosols or cloud droplets through molecular diffusion and free collision is  
144 given by

$$145 \quad k = \left( \frac{a}{D_g} + \frac{4}{v\gamma} \right)^{-1} A \quad (1)$$

146 where  $D_g$  is the gas-phase molecular diffusion coefficient,  $a$  is the radius of the aerosol particle or  
147 cloud droplet,  $v$  is the mean molecular speed,  $\gamma$  is the reaction uptake coefficient when a collision  
148 occurs between a gas-phase molecule and the aqueous surface, and  $A$  is the aqueous particle surface  
149 area per unit volume of air.

150 We implement the reactive uptake of dicarbonyls by cloud droplets following the standard

151 equation (1). In a similar manner to Fu et al. (2008) and Li et al. (2013), the cloud droplet surface  
152 area is calculated from the LWC in the cloudy fraction of the model grid by assuming an effective  
153 droplet radius of 6  $\mu\text{m}$  for continental clouds and 10  $\mu\text{m}$  for maritime clouds.  $D_g$  is calculated  
154 according to Perry and Green (1999) following Dentener and Crutzen (1993). Similar to previous  
155 studies (e.g. Lin et al., 2014; Ying et al., 2015; Hu et al., 2017), the uptake of gas-phase dicarbonyls  
156 on aqueous aerosols is simply parameterized using the collision limitation ( $v\gamma A/4$ ) of equation (1).  
157 The value of  $\gamma = 2.9 \times 10^{-3}$  for glyoxal from Liggio et al. (2005) is used in both cloud and aerosol  
158 processing. While the uptake coefficient adopted for methylglyoxal is from De Haan et al. (2018):  
159 the average value of  $\gamma = 5.7 \times 10^{-3}$  measured on cloud-processed glycine aerosols is used to account  
160 for the uptake by cloud droplets; the average value of  $\gamma = 3.0 \times 10^{-3}$  used in aerosol processing is  
161 derived from the uptake coefficients measured on deliquesced ammonium sulfate aerosols ( $3.7 \times 10^{-3}$ )  
162 and on deliquesced glycine aerosols ( $2.3 \times 10^{-3}$ , median value).

163

### 164 **2.3 Observational data**

165 To assess the contribution of dicarbonyl species to the concentration of SOA, we used the observed  
166 hourly concentration of SOA in Beijing during the summer and fall of 2014 measured by Xu et al.  
167 (2017) with an Aerodyne high-resolution time-of-flight aerosol mass spectrometer. Samples were  
168 taken from June 3 to July 11, 2014 (episode 1) and October 14 to November 14, 2014 (episode 2)  
169 at the Institute of Atmospheric Physics. More detailed information about the data has been reported  
170 by Xu et al. (2017). The simulation periods are from May 22 to July 11 and from October 1 to  
171 November 14, with the first 12 days as the spin-up time. To evaluate the reasonability in simulating  
172 the formation processes of aqueous SOAs and analyze the relative causes, the corresponding cloud  
173 water path (CWP) and cloud fraction data measured by the MODerate Resolution Imaging  
174 Spectroradiometer (MODIS) was obtained from the website [http://ladsweb.modaps.eosdis.nas  
175 a.gov/api/v1/productPage/product=MYDATML2](http://ladsweb.modaps.eosdis.nasa.gov/api/v1/productPage/product=MYDATML2), and the observed precipitation data was  
176 downloaded from the website <http://chrsdata.eng.uci.edu/>.

177 Both Liu et al. (2012) and Li et al. (2018) have suggested that the underestimation of glyoxal  
178 concentrations in simulations is related to the underpredicted emission of aromatic compounds.  
179 Therefore, the biases in the emission of aromatic compounds need to be evaluated through a  
180 comparison of the observed and simulated concentrations of aromatic compounds. The observed

181 data was collected at 14:00 local standard time every Thursday by gas chromatography–mass  
182 spectrometer at Beijing, Xinglong and Yucheng (Fig. 1). Sun et al. (2016) and Wu et al. (2016) have  
183 presented the detailed information.

184 To evaluate the performance of our model, we also compared the simulated PM<sub>2.5</sub> concentrations  
185 and several meteorological factors with the results measured over 12 stations (Fig. 1) during the two  
186 episodes. The observed meteorological data was derived from the Meteorological Information  
187 Comprehensive Analysis and Process System (MICAPS) dataset, whereas the Chinese National  
188 Environmental Monitoring Center provided the measured concentrations of PM<sub>2.5</sub>.

189

### 190 **3. Results and discussions**

#### 191 **3.1 Base model evaluation**

192 Table 1 shows statistical results of the meteorological parameters (i.e. temperature, relative humidity,  
193 wind speed and wind direction) and PM<sub>2.5</sub> concentrations in the two analyzed episodes, where:  $N$  is  
194 the total number of samples; IOA is the index of agreement, which can synthetically reflect the  
195 combination of the modeled value and variable tendency being good or bad (Willmott, 1981);  $C_{\text{mod}}$   
196 and  $C_{\text{obs}}$  are the average values of modeled and observed results, respectively; MB and FB are the  
197 mean and fractional bias, respectively; RMSE and FE are the root-mean-square and fractional error,  
198 respectively; and  $R$  is the correlation coefficient between the observed and simulated results. The  
199 calculations of these statistical parameters can be found in Juda-Rezler et al. (2012).  $P_{22.5^\circ}$  and  $P_{45^\circ}$   
200 represent the proportions of compared results that the absolute biases between the simulated and  
201 measured wind directions are within  $22.5^\circ$  and  $45^\circ$ , respectively (Li et al., 2017a).

202 There are inevitably some biases in the simulated meteorological parameters relative to the  
203 observations due to the limited model resolution and system errors. Nevertheless, the model  
204 reproduces the magnitude and variation trend of the temperature and relative humidity fairly well  
205 (Figs. S1 and S2), with IOAs for temperature of 0.91 and 0.95 in the two episodes and IOAs of 0.91  
206 and 0.88 for the relative humidity, comparable with the results of Li et al. (2012) and Wang et al.  
207 (2014). The mean biases of temperature ( $-0.83^\circ\text{C}$ ,  $-0.68^\circ\text{C}$ ) and relative humidity (1.53%,  $-0.05\%$ )  
208 are small in the two episodes. The RMSEs of temperature and relative humidity are comparable  
209 with the results of Gao et al. (2016) and Zhang et al. (2012), implying a reasonable performance of  
210 the simulation. Although the capture of the variable tendency of wind speed (Fig. S3) by the model

211 is rather poor, the small values for the mean bias ( $-0.40$  and  $-0.22$  m/s) and the high IOAs (0.61 and  
212 0.69) indicate a better performance than that reported by Feng et al. (2016) and Wang et al. (2014)  
213 in simulating the wind speed. The RMSE of wind speed shows that the simulated results achieve  
214 the criteria for a good performance ( $|\text{RMSE}| \leq 2$  m/s) given by Emery et al. (2001). For the wind  
215 direction (Fig. S4),  $P_{22.5^\circ}$  and  $P_{45^\circ}$  are 32.12 and 54.52% in episode 1 and 34.01 and 57.41% in  
216 episode 2, indicating the reasonable simulation of wind direction. Therefore the model provides a  
217 reasonable meteorological field for the subsequent simulations.

218 The modeled  $\text{PM}_{2.5}$  concentrations are generally higher than the observed values in the two  
219 episodes over the 12 stations (Fig. S5). Except for the limited resolution of the model, the  
220 uncertainties of the emission inventory and the effects of the background transport may also  
221 contribute to the overestimation. However, the correlation coefficients of  $\text{PM}_{2.5}$  are 0.50 and 0.56 in  
222 the two episodes, respectively, and the IOAs are 0.64 and 0.70 in the two episodes, respectively,  
223 indicating good capture of the variable tendency and magnitude by the model. Both the fractional  
224 error and the fractional bias for  $\text{PM}_{2.5}$  in the two episodes fulfill the performance criteria ( $\text{FE} \leq 75\%$ ,  
225  $|\text{FB}| \leq 60\%$ ) given by Boylan and Russell (2006), implying a good performance in simulating  $\text{PM}_{2.5}$ .  
226 These results show that the model gives a reasonable simulation of the chemical species.

227 The modeled and satellite-observed mean CWP were compared in Fig. 2 during the two analyzed  
228 episodes to evaluate the reasonability in simulating the aqueous SOA formations. Fig. 2a and 2b  
229 show that in episode 1, during one summer period, the highest observed CWP ( $400\text{--}500$  g/m<sup>2</sup>)  
230 mainly appears over the Yellow Sea and Bohai Sea and in parts of southeastern and southern China,  
231 whereas the observed second highest values ( $200\text{--}300$  g/m<sup>2</sup>) are concentrated in from the Qinghai–  
232 Tibetan Plateau to the North China Plain along the Yellow River Basin. The modeled high CWP  
233 ( $100\text{--}400$  g/m<sup>2</sup>) appears in the same regions as in the observational dataset. In episode 2, during one  
234 fall period (Fig. 2c and 2d), the observed highest ( $300\text{--}500$  g/m<sup>2</sup>) and second highest ( $200\text{--}300$  g/m<sup>2</sup>)  
235 CWP values are mainly concentrated in the Hetao area and the regions including the northeastern  
236 China and Inner Mongolia, respectively. The modeled values ( $50\text{--}150$  g/m<sup>2</sup>) are also high over these  
237 regions.

238 Overall, there are obvious biases in the numerical values between the observed and simulated  
239 CWP. According to the comparisons between the observed and modeled cloud fraction and  
240 precipitation (shown in Fig. S6 and S7), this is a result that has a lot to do with the uncertainties in



241 the cloud fraction estimations, which indirectly lead to uncertainties in the simulations of the  
242 concentrations of SOAs. However, the mean distribution patterns of the simulated CWP during the  
243 two episodes are similar to the observational results, indicating few impacts on the simulated  
244 distribution of SOA. Both the simulated and observed CWP in episode 1 are higher than in episode  
245 2, also implying differences in the simulation of SOA between the two episodes.

246

### 247 **3.2 Model results and analyses**

248 As described in Section 2.3 and with reference to previous research, the underestimation of glyoxal  
249 concentrations may partly result from the underprediction of the emissions of aromatic compounds.  
250 It is therefore necessary to evaluate the emissions of aromatic compounds during the analyzed  
251 episodes with the base model before designing and implementing the sensitivity case studies. For  
252 this purpose, comparisons were made between the simulated and observed concentrations of  
253 aromatic compounds in a similar manner to the work of Zhang and Ying (2011).

254 Fig. 3 presents the ratio of the observed to predicted (O/P ratio) concentrations of aromatic  
255 compounds for the original emissions (Fig. 3a and 3c) and a three-fold increase in the emissions of  
256 aromatic compounds (Fig. 3b and 3d) during the two episodes. Fig. 3a shows that there are biases  
257 between the observed and simulated concentrations of aromatic compounds in episode 1 at the  
258 original emission rates of the aromatic compounds. The O/P ratios are less variable for ARO1 than  
259 for ARO2, with both the mean and median O/P values being close to 2. The range of O/P values is  
260 large for ARO2 and there is an order of magnitude difference between the lowest and highest ratios.  
261 Both the mean and median O/P ratios of ARO2 are about 20. These results show that there are  
262 underestimations in the emissions of ARO1 and ARO2. In view of the limitations of the amount of  
263 observed data and the nonlinear relationship between emissions and the concentrations (Li et al.,  
264 2018), the underestimation in the emission rates has been conservatively estimated to be a factor of  
265 three. As a result, when the emission rates of aromatic compounds are increased (Fig. 3b), the ratios  
266 of ARO1 and ARO2 in episode 1 are less variable, especially ARO2. The mean and median ratios  
267 of ARO1 are both around 1, whereas the two ratios for ARO2 decrease from 20 to 6. The results for  
268 episode 2 are similar to those in episode 1. Fig. 3c shows that the original O/P ratio of ARO1 varies  
269 between 1 and 3.5, with a mean value close to 2, whereas the ratio of ARO2 ranges from 1 to 5, with  
270 a mean ratio of about 4, both of which indicate unaccounted emissions of aromatic compounds. Fig.

271 3d shows a clear decrease in the biases of the observed and simulated concentrations of aromatic  
272 compounds. The O/P ratios of ARO1 and ARO2 are concentrated and vary between 1 and 2, with a  
273 mean ratio close to 1. However, it is difficult to determine whether the factor of 3 is the actual  
274 underestimation in the emission of aromatic compounds as a result of its dependence on space and  
275 time. For convenience, a factor of 3 is chosen here as a uniform scale with which to assess the  
276 unaccounted emissions of aromatic compounds.

277 Three sensitivity simulation case studies are designed based on these results. Case 0 is run with  
278 the three default SOA formation pathways included in the standard model. According to Fu et al.  
279 (2008), the default aqueous SOA formation pathway is included in the pathway M. To avoid double-  
280 counting the loss of dicarbonyls through the in-cloud oxidation and the following formed SOA, the  
281 default aqueous SOA formation pathway is turned off when run case 1 with the pathway M  
282 incorporated. According to previous studies (e.g. Stavrakou et al., 2009; Stavrakou et al., 2010; Li et  
283 al., 2016), the yields of glyoxal from isoprene are very likely to be underestimated. Li et al. (2018)  
284 has run a simple sensitivity case to evaluate the impacts of underestimated glyoxal yields from  
285 isoprene on glyoxal simulation. From their results, a better agreement has achieved between the  
286 observed and simulated glyoxal after a five-fold increase of glyoxal yields from isoprene. More  
287 detailed analyses can be found in Li et al. (2018). Thus, to take the effects of the underestimations  
288 of glyoxal concentrations into considerations, case 2 is designed with a three-fold increase in the  
289 emissions of aromatic compounds and a five-fold increase in the molar yield of glyoxal from  
290 isoprene based on the results of case 1.

291 Fig. 4 compares the hourly concentrations of the simulated and observed SOAs during the two  
292 analyzed episodes; the corresponding statistical parameters are listed in Table 2. The concentrations  
293 of SOAs are measured from PM<sub>1</sub>. The observed PM<sub>1</sub>/PM<sub>2.5</sub> ratio of 0.77 (Xu et al., 2015) was used  
294 to convert the observed concentrations for comparison with the simulated results for PM<sub>2.5</sub>.

295 In case 0, the SOA concentrations in episode 1 (Fig. 4a) are significantly underestimated by an  
296 average factor of 5.7, with the differences being as high as a multiple of  $\geq 60$ . As a result of the  
297 impacts of uncertainties in the meteorological fields and emissions, the variation trend of the  
298 concentration of SOA is not well captured by the model ( $R = 0.21$ ). Similarly, although the variation  
299 of SOA is reproduced well in episode 2 ( $R = 0.83$ ) (Fig. 4b), the concentration of SOA is still  
300 underpredicted by an order of magnitude. The biases between the observed and simulated

301 concentrations of SOAs decrease in case 1 when pathway M is added to the model, especially in  
302 episode 1. It shows that the mean concentration of SOA in case 1 increases by  $3.65 \mu\text{g}/\text{m}^3$  during  
303 episode 1, explaining 34.8% of the unaccounted sources of SOAs. The decreased mean bias and  
304 RMSE and the slightly increased IOA also indicate the more reasonable descriptions of the  
305 formations of SOAs. In episode 2, the SOA formed through pathway M contributes less to the total  
306 concentration of SOA. The mean SOA concentration during episode 2 reaches  $2.87 \mu\text{g}/\text{m}^3$ , increased  
307 by  $1.82 \mu\text{g}/\text{m}^3$ . However, the decreased bias statistical parameters (e.g. RMSE and MB) also indicate  
308 the more realistic description of contributions of dicarbonyls to SOA in this episode. The larger  
309 contribution of dicarbonyls from pathway M to the concentration of SOA in episode 1 is attributed  
310 to the higher LWC and the larger amount of dicarbonyls produced from biogenic precursors in the  
311 summer than in the fall. When the impact of the underestimation of glyoxal on the concentration of  
312 SOA is further taken into consideration, the concentration of SOA clearly increases in case 2.  
313 Compared to case 0, the mean concentration of SOA in episode 1 is significantly improved by a  
314 factor of 5.4 and comparable to the observations, whereas the increase in episode 2 is a factor of 6.2.  
315 The statistical parameters (e.g. IOA and RMSE) also show the better performance of case 2,  
316 indicating a more realistic and reasonable representation of the formation of SOA. Aromatic  
317 compounds are not only the precursors of glyoxal, but are also the precursors of SOA in the gas  
318 phase. A compositional analysis is therefore required to evaluate the individual contributions from  
319 dicarbonyls in case 2.

320 Fig. 5 shows the mean contributions from different sources of SOAs in the three sensitivity case  
321 studies during the two analyzed episodes. AAQ, dicarbonyl-derived SOAs, contributes little in case  
322 0 during the two episodes. The mean contribution of AAQ to the total concentration of SOAs in  
323 episode 1 is 2.39%, larger than in episode 2 (0.89%). As a result of the greater amount of emissions  
324 from biogenic sources in summer, SOAs formed from biogenic precursors (AISOP+ATRP+ASQT)  
325 contribute more (26.3%) in episode 1 than that in episode 2 (13.5%), whereas the contributions from  
326 anthropogenic precursors (AALK+ATOL+AXYL+ABNZ) are comparable between the two  
327 episodes. When pathway M is included in the model, the contribution from AAQ to SOA in case 1  
328 clearly increases and reaches 57.1% in episode 1 and 63.7% in episode 2. The significant  
329 contributions from AAQ in the two episodes indicate the major contributions from dicarbonyls  
330 through pathway M to the formations of SOAs in summer and fall. When the impact of the

331 underestimation of glyoxal is further taken into consideration in case 2, the mean concentration of  
332 AAQ in both episodes are higher than double that of case 1. In episode 1, AAQ ( $7.29 \mu\text{g}/\text{m}^3$ )  
333 accounts for 60.6% of the total SOA, exceeding the sum of the contributions from ARO1 (ATOL)  
334 and ARO2 (AXYL) (16.0%), and indicating the dominant contribution of aqueous-phase process to  
335 the concentration of SOA in summer. The increase in AAQ relative to case 0 compensates for about  
336 69.1% of the unaccounted sources of SOAs. In episode 2, AAQ ( $4.21 \mu\text{g}/\text{m}^3$ ) contributes 64.5% to  
337 the total concentration of SOA, which is also higher than the sum of ATOL and AXYL (15.3%),  
338 implying the dominant contributions of dicarbonyls to the concentrations of SOAs. The different  
339 contribution of AAQ in case 2 during the two episodes can be attributed to the different LWC and  
340 different amount of dicarbonyls produced from biogenic precursors.

341 It is clear that the biases between the observed and simulated concentrations of SOAs decrease  
342 when the contributions of unaccounted dicarbonyls to the concentrations of SOAs are considered,  
343 especially in summer. However, the sources of unaccounted SOAs cannot be explained completely.  
344 As a result of uncertainties in the description of known SOA formation processes and missing  
345 pathways that are not included in the model—for example, there are many uncertainties in glyoxal  
346 simulations (Li et al. (2018)). There are also many uncertainties in incorporating pathway M into  
347 the model, such as the effective radius of cloud droplets (the empirical values used instead of the  
348 actual values), the reaction uptake coefficient (updated values over disparate surfaces are discussed  
349 in Curry et al. (2018)), and the liquid water content in clouds (the most uncertain parameter). Other  
350 pathways for the formations of SOAs, such as the uptake of isoprene epoxides on the surface of  
351 aerosols (Lal et al., 2012; Lin et al., 2013), the aging mechanism of semi-volatile primary organic  
352 aerosols (Shrivastava et al., 2008) and the oxidation of primary semi- and intermediate VOCs, are  
353 not considered in this model. Besides, recent studies (e.g. Galloway et al., 2009; De Haan et al., 2018)  
354 have presented that the reactive uptake of glyoxal and methylglyoxal can be reversible, especially  
355 methylglyoxal, but we do not consider in this study.

356 To distinguish the contribution of dicarbonyls to the concentration of SOA over China in case 2  
357 from that in case 0, the distributions of dicarbonyl-derived SOAs and their contributions to SOAs  
358 (AAQ/SOA) over China in cases 0 and 2 are analyzed.

359 Fig. 6(a, b) and 6(c, d) show the mean concentration of AAQ in cases 0 and 2, respectively, during  
360 the two episodes. For the base case, in episode 1 (Fig. 6a), the concentration of AAQ over China is

361  $\leq 0.2 \mu\text{g}/\text{m}^3$ . The higher concentration of AAQ ( $0.1\text{--}0.2 \mu\text{g}/\text{m}^3$ ) is in the areas between the lower  
362 reaches of the Yellow and Yangtze rivers and in the Sichuan Basin, probably due to the higher LWC  
363 and a greater number of sources of dicarbonyls over these areas, as discussed in Section 3.1 and by  
364 Li et al. (2018). While in episode 2 (Fig. 6b), the concentration of AAQ is  $\leq 0.1 \mu\text{g}/\text{m}^3$  over the  
365 regions for the lower LWC and less sources of dicarbonyls from biogenic precursors. It is clear that  
366 the concentration of AAQ is improved in case 2, when pathway M is added and the impact of the  
367 underestimation of glyoxal is considered. Overall, the concentration of AAQ is higher in eastern  
368 China than in the west during the two episodes. In episode 1 (Fig. 6c), the concentrations of AAQ  
369 mostly vary from 2 to  $15 \mu\text{g}/\text{m}^3$  over central and eastern China, with the highest value ( $10\text{--}15 \mu\text{g}/\text{m}^3$ )  
370 concentrated in the areas over the lower reaches of the Yangtze river. The concentration of AAQ in  
371 western China is  $\leq 1 \mu\text{g}/\text{m}^3$ , with the lowest value ( $\leq 0.1 \mu\text{g}/\text{m}^3$ ) in the Qinghai-Tibet Plateau,  
372 probably because there are few sources of dicarbonyls. In episode 2 (Fig. 6d), the concentrations of  
373 AAQ is mostly in a range of  $2\text{--}10 \mu\text{g}/\text{m}^3$  over central and eastern China, with the highest value ( $5\text{--}$   
374  $10 \mu\text{g}/\text{m}^3$ ) concentrated over regions from south of the lower reaches of the Yellow River to the  
375 south of Guangzhou Province as well as the Sichuan Basin. The concentration of AAQ in western  
376 China is also  $\leq 1 \mu\text{g}/\text{m}^3$ , with the lowest value ( $\leq 0.1 \mu\text{g}/\text{m}^3$ ) in the Qinghai-Tibet Plateau. Outside  
377 China, the highest concentration of AAQ (15-20) appears in the northeastern India due to more  
378 primary sources of dicarbonyls from the large scale of postharvest paddy residue burnings (Chandra  
379 and Sinha, 2016) and the barrier of precursor gases diffusions from Himalayan orogen as well as  
380 the low wind speed.

381 Fig. 6(e, f) and 6(g, h) show the spatial distribution of the mean AAQ/SOA in cases 0 and 2 during  
382 the two episodes, respectively. Fig. 6e shows that the AAQ fraction over China in episode 1 is  $\leq$   
383 10%, except in Yunnan Province and some parts of the South China Sea, where AAQ/SOA reaches  
384 10–20%. In episode 2 (Fig. 6f), the mean AAQ/SOA is  $\leq 10\%$  over the whole regions. When the  
385 contributions of dicarbonyls from pathway M and improved glyoxal to SOA are considered, there  
386 is a large increase in AAQ/SOA over these regions in two episodes. As shown in Fig. 6g, in episode  
387 1, the contribution of AAQ to SOA varies from 10 to 90% throughout China. In central and eastern  
388 areas, the fraction of AAQ is generally in the range of 50–70% and up to 70–90% in the coastal  
389 regions and offshore from the East China Sea to the South China Sea. The fraction of AAQ in the  
390 west is relatively low and usually  $\leq 50\%$ . However, the contribution of AAQ to SOA is up to 80%

391 in southwestern regions (e.g. Yunnan Province and parts of Sichuan Province). In episode 2 (Fig.  
392 6h), the contribution of AAQ to SOA is in the range of 10–80% throughout China. In central and  
393 eastern areas, the fraction of AAQ is generally in the range of 50–70% and up 80% in a small portion  
394 of northeastern China. The fraction of AAQ in the west is also lower and usually  $\leq 50\%$ . However,  
395 the contribution of AAQ to SOA is up to 60-70% in a small part of Sinkiang Province.

#### 396 **4. Conclusions**

397 The RAMS-CMAQ modeling system was used to assess the contributions of dicarbonyls from the  
398 reactive uptake process and unaccounted sources of glyoxal to the concentrations of SOAs during  
399 the two episodes from June 3 to July 11, 2014 and October 14 to November 14, 2014. Comparisons  
400 between the observed and simulated concentrations of SOAs from three sensitivity groups showed  
401 different improvements in the SOA simulations with the inclusion of pathway M and consideration  
402 of the underestimation of glyoxal in the two episodes. Due to the high LWC and large amount of  
403 dicarbonyls produced from biogenic precursors in summer, the contributions of dicarbonyls were  
404 greater in episode 1 than that in episode 2. When pathway M was added in case 1, the modeled mean  
405 concentration of SOA in episode 1 increased by  $3.65 \mu\text{g}/\text{m}^3$ , explaining about 34.8% of the  
406 unaccounted SOA sources, while there was a  $1.82 \mu\text{g}/\text{m}^3$  increase in the mean result during episode  
407 2. When the impacts of glyoxal underestimation were further taken into consideration in case 2, the  
408 modeled mean AAQ in episode 1 was improved to  $7.29 \mu\text{g}/\text{m}^3$  and contributed 60.6% of the total  
409 concentration of SOA. The increase due to AAQ relative to case 0 is equivalent to 69.1% of the  
410 unaccounted source of SOA. Whereas the mean concentration of AAQ in episode 2 was  $4.21 \mu\text{g}/\text{m}^3$   
411 and accounted for 64.5% of total concentration of SOA. Although the contributions of dicarbonyls  
412 to SOAs are different in the two episodes, the simulated SOA results are both improved and close  
413 to the observations, indicating a more realistic description of aqueous SOA formation.

414 The mean AAQ in case 2 during the two episodes was clearly improved over China relative to  
415 case 0 and was generally higher in the east than in the west. In episode 1, the highest value ( $10\text{--}15$   
416  $\mu\text{g}/\text{m}^3$ ) was seen in the areas around the lower reaches of the Yellow River. While the highest value  
417 ( $5\text{--}10 \mu\text{g}/\text{m}^3$ ) in episode 2 was concentrated over regions from south of the lower reaches of the  
418 Yellow River to the south of Guangzhou Province as well as the Sichuan Basin. As a result, the  
419 contribution of AAQ to the concentration of SOA in two episodes was also improved in case 2. In  
420 episode 1, the fraction varied from 10 to 90% throughout China, with the highest contribution (70–

421 90%) in the coastal regions and offshore along the East China Sea to the South China Sea in addition  
422 to the southwestern regions (e.g. Yunnan Province and parts of Sichuan Province). While in episode  
423 2, the contribution of AAQ to SOA was in the range of 10–80% throughout China, with the highest  
424 fraction (up to 80%) seen in a small portion of northeastern China.

425 It is clear that the contributions of dicarbonyls from pathway M and the unaccounted sources of  
426 glyoxal make a significant contribution to the concentration of SOA, especially in summer. However,  
427 there are still many uncertainties in the depictions of reactive uptake processes and sources of  
428 glyoxal. For example, the reactive uptake of dicarbonyls in this study has been processed as  
429 irreversible reactions. However, several recent studies (e.g. Galloway et al., 2009; De Haan et al.,  
430 2018) have presented that the uptake processes can be reversible, but we do not consider. For another  
431 example, the uptake coefficient of dicarbonyls has been reported to vary between different surfaces  
432 by Curry et al. (2018), including the differences between the cloud droplet and aqueous aerosol and  
433 between each aerosol components. But we do not make the distinctions. What's more, the liquid  
434 water content which is not well reproduced in the model, the effective radius of cloud droplets which  
435 are the fixed empirical values used instead of the actual values, and the evaluations of the  
436 underestimations in the aromatic compound emissions which are not well discussed due to the  
437 limited observed data can also bring the uncertainties into our results. Thus, more work about the  
438 dicarbonyl-derived SOA need to be done in future.

439 Besides, the aqueous SOA formation is not only relative to the distributions of dicarbonyl  
440 concentrations, but also depends on the liquid water content (LWC). Due to the large space and time  
441 dependence, one single station measurement of SOA concentration is not enough to evaluate the  
442 model performance over China, especially the impacts of glyoxal underestimations on dicarbonyl-  
443 derived SOA. Thus, more observed SOA data from different stations need to be collected and used  
444 for comparisons to reduce the uncertainties in the conclusions.

445

446 *Author contribution.* In this study, J. Li designed the sensitivity experiments, developed the model code, and  
447 performed the corresponding simulations. M. Zhang co-designed the experiments and provided valuable advices  
448 about the model operations. Y. Sun carried out the measurements of SOA and provided the corresponding data for  
449 evaluating the modeled results. G. Tang and F. Wu carried out the measurements of aromatic compound  
450 concentrations and provided the corresponding data for evaluating the simulated results. Y. Xu provided valuable

451 advice on model result analysis.

452

453 *Acknowledgments.* This study was supported by the National Key R&D Programs of China (No. 2017YFC0209803),  
454 the National Natural Science Foundation of China (91544221), and the Beijing Municipal Science and Technology  
455 Project (ZL171100000617002). We thank Professor Qi Ying for helping to incorporate the reactive uptake of  
456 dicarbonyls pathway into the model.

457

## 458 **References**

- 459 Benkovitz, C. M., Scholtz, M. T., Pacyna, J., Tarrason, L., Dignon, J., Voldner, E. C., Spiro, P. A., Logan, J. A., and  
460 Graedel, T. E.: Global gridded inventories of anthropogenic emissions of sulfur and nitrogen, *J. Geophys. Res.-*  
461 *Atmos.*, 101, 29239-29253, 10.1029/96jd00126, 1996.
- 462 Boylan, J. W., and Russell, A. G.: PM and light extinction model performance metrics, goals, and criteria for three-  
463 dimensional air quality models, *Atmos. Environ.*, 40, 4946-4959, 10.1016/j.atmosenv.2005.09.087, 2006.
- 464 Byun, D., and Schere, K. L.: Review of the governing equations, computational algorithms, and other components  
465 of the models-3 Community Multiscale Air Quality (CMAQ) modeling system, *Applied Mechanics Reviews*, 59,  
466 51-77, 10.1115/1.2128636, 2006.
- 467 Carlton, A. G., Turpin, B. J., Lim, H. J., Altieri, K. E., and Seitzinger, S.: Link between isoprene and secondary  
468 organic aerosol (SOA): Pyruvic acid oxidation yields low volatility organic acids in clouds, *Geophys. Res. Lett.*,  
469 33, 272-288, 2006.
- 470 Carlton, A. G., Turpin, B. J., Altieri, K. E., Seitzinger, S. P., Mathur, R., Roselle, S. J., and Weber, R. J.: CMAQ  
471 Model Performance Enhanced When In-Cloud Secondary Organic Aerosol is Included: Comparisons of Organic  
472 Carbon Predictions with Measurements, *Environ. Sci. Technol.*, 42, 8798-8802, 10.1021/es801192n, 2008.
- 473 Carlton, A. G., Bhave, P. V., Napelenok, S. L., Edney, E. D., Sarwar, G., Pinder, R. W., Pouliot, G. A., and Houyoux,  
474 M.: Model Representation of Secondary Organic Aerosol in CMAQv4.7, *Environ. Sci. Technol.*, 44, 8553-8560,  
475 10.1021/es100636q, 2010.
- 476 Carter, W. P. L.: Implementation of the SAPRC-99 Chemical Mechanism into the Models-3 Framework Report to  
477 the US Environmental Protection Agency, Research Triangle Park, NC, 2000.
- 478 Chandra, B. P., and Sinha, V.: Contribution of post-harvest agricultural paddy residue fires in the NW Indo-Gangetic  
479 Plain to ambient carcinogenic benzenoids, toxic isocyanic acid and carbon monoxide, *Environment International*,  
480 88, 187-197, 10.1016/j.envint.2015.12.025, 2016.
- 481 Corrigan, A. L., Hanley, S. W., and De Haan, D. O.: Uptake of glyoxal by organic and inorganic aerosol, *Environ.*  
482 *Sci. Technol.*, 42, 4428-4433, 10.1021/es7032394, 2008.
- 483 Cotton, W. R., Pielke, R. A., Walko, R. L., Liston, G. E., Tremback, C. J., Jiang, H., McAnelly, R. L., Harrington, J.  
484 Y., Nicholls, M. E., Carrio, G. G., and McFadden, J. P.: RAMS 2001: Current status and future directions, *Meteorol.*  
485 *Atmos. Phys.*, 82, 5-29, 10.1007/s00703-001-0584-9, 2003.
- 486 Curry, L. A., Tsui, W. G., and McNeill, V. F.: Technical note: Updated parameterization of the reactive uptake of  
487 glyoxal and methylglyoxal by atmospheric aerosols and cloud droplets, *Atmos. Chem. Phys.*, 18, 9823-9830,  
488 10.5194/acp-18-9823-2018, 2018.
- 489 de Gouw, J. A., Middlebrook, A. M., Warneke, C., Goldan, P. D., Kuster, W. C., Roberts, J. M., Fehsenfeld, F. C.,  
490 Worsnop, D. R., Canagaratna, M. R., Pszenny, A. A. P., Keene, W. C., Marchewka, M., Bertman, S. B., and Bates,  
491 T. S.: Budget of organic carbon in a polluted atmosphere: Results from the New England Air Quality Study in



492 2002, *J. Geophys. Res.-Atmos.*, 110, 10.1029/2004jd005623, 2005.

493 Emery, C., Tai, E., Yarwood, G.: Enhanced meteorological modeling and performance evaluation for two Texas  
494 ozone episodes, In: Prepared for the Texas Natural Resource Conservation Commission, ENVIRON International  
495 Corporation, Novato, CA, USA, 2001.

496 De Haan, D. O., Jimenez, N. G., de Loera, A., Cazaunau, M., Gratien, A., Pangui, E., and Doussin, J.-F.:  
497 Methylglyoxal Uptake Coefficients on Aqueous Aerosol Surfaces, *The Journal of Physical Chemistry A*, 122,  
498 4854-4860, 10.1021/acs.jpca.8b00533, 2018.

499 Dentener, F. J., and Crutzen, P. J.: REACTION OF N<sub>2</sub>O<sub>5</sub> ON TROPOSPHERIC AEROSOLS - IMPACT ON THE  
500 GLOBAL DISTRIBUTIONS OF NO<sub>x</sub>, O<sub>3</sub>, AND OH, *J. Geophys. Res.-Atmos.*, 98, 7149-7163,  
501 10.1029/92jd02979, 1993.

502 Emmons, L. K., Walters, S., Hess, P. G., Lamarque, J. F., Pfister, G. G., Fillmore, D., Granier, C., Guenther, A.,  
503 Kinnison, D., Laepple, T., Orlando, J., Tie, X., Tyndall, G., Wiedinmyer, C., Baughcum, S. L., and Kloster, S.:  
504 Description and evaluation of the Model for Ozone and Related chemical Tracers, version 4 (MOZART-4), *Geosci.*  
505 *Model Dev.*, 3, 43-67, 2010.

506 Ervens, B., Feingold, G., Frost, G. J., and Kreidenweis, S. M.: A modeling study of aqueous production of  
507 dicarboxylic acids: 1. Chemical pathways and speciated organic mass production, *J. Geophys. Res.: Atmos.*, 109,  
508 D15205, 10.1029/2003JD004387, 2004.

509 Ervens, B., and Volkamer, R.: Glyoxal processing by aerosol multiphase chemistry: towards a kinetic modeling  
510 framework of secondary organic aerosol formation in aqueous particles, *Atmos. Chem. Phys.*, 10, 8219-8244,  
511 10.5194/acp-10-8219-2010, 2010.

512 Ervens, B., Turpin, B. J., and Weber, R. J.: Secondary organic aerosol formation in cloud droplets and aqueous  
513 particles (aqSOA): a review of laboratory, field and model studies, *Atmos. Chem. Phys.*, 11, 11069-11102,  
514 10.5194/acp-11-11069-2011, 2011.

515 Ervens, B., Sorooshian, A., Lim, Y. B., and Turpin, B. J.: Key parameters controlling OH-initiated formation of  
516 secondary organic aerosol in the aqueous phase (aqSOA), *J. Geophys. Res.-Atmos.*, 119, 3997-4016,  
517 10.1002/2013jd021021, 2014.

518 Farina, S. C., Adams, P. J., and Pandis, S. N.: Modeling global secondary organic aerosol formation and processing  
519 with the volatility basis set: Implications for anthropogenic secondary organic aerosol, *J. Geophys. Res.-Atmos.*,  
520 115, 10.1029/2009jd013046, 2010.

521 Feng, T., Bei, N., Huang, R.-J., Cao, J., Zhang, Q., Zhou, W., Tie, X., Liu, S., Zhang, T., Su, X., Lei, W., Molina, L.  
522 T., and Li, G.: Summertime ozone formation in Xi'an and surrounding areas, China, *Atmos. Chem. Phys.*, 16,  
523 4323-4342, 10.5194/acp-16-4323-2016, 2016.

524 Foley, K. M., Roselle, S. J., Appel, K. W., Bhawe, P. V., Pleim, J. E., Otte, T. L., Mathur, R., Sarwar, G., Young, J.  
525 O., Gilliam, R. C., Nolte, C. G., Kelly, J. T., Gilliland, A. B., and Bash, J. O.: Incremental testing of the Community  
526 Multiscale Air Quality (CMAQ) modeling system version 4.7, *Geosci. Model Dev.*, 3, 205-226, 10.5194/gmd-3-  
527 205-2010, 2010.

528 Fu, T.-M., Jacob, D. J., Wittrock, F., Burrows, J. P., Vrekoussis, M., and Henze, D. K.: Global budgets of atmospheric  
529 glyoxal and methylglyoxal, and implications for formation of secondary organic aerosols, *J. Geophys. Res.-*  
530 *Atmos.*, 113, 10.1029/2007jd009505, 2008.

531 Fu, T. M., Jacob, D. J., and Heald, C. L.: Aqueous-phase reactive uptake of dicarbonyls as a source of organic aerosol  
532 over eastern North America, *Atmos. Environ.*, 43, 1814-1822, 2009.

533 Galloway, M. M., Chhabra, P. S., Chan, A. W. H., Surratt, J. D., Flagan, R. C., Seinfeld, J. H., and Keutsch, F. N.:  
534 Glyoxal uptake on ammonium sulphate seed aerosol: reaction products and reversibility of uptake under dark and  
535 irradiated conditions, *Atmos. Chem. Phys.*, 9, 3331-3345, 10.5194/acp-9-3331-2009, 2009.

536 Gao, M., Carmichael, G. R., Wang, Y., Saide, P. E., Yu, M., Xin, J., Liu, Z., and Wang, Z.: Modeling study of the  
537 2010 regional haze event in the North China Plain, *Atmos. Chem. Phys.*, 16, 1673-1691, 10.5194/acp-16-1673-  
538 2016, 2016.

539 Goldstein, A. H., and Galbally, I. E.: Known and unexplored organic constituents in the earth's atmosphere, *Environ.*  
540 *Sci. Technol.*, 41, 1514-1521, 10.1021/es072476p, 2007.

541 Gong, S. L.: A parameterization of sea-salt aerosol source function for sub- and super-micron particles, *Global*  
542 *Biogeochem. Cycles*, 17, 10.1029/2003gb002079, 2003.

543 Guenther, A. B., Jiang, X., Heald, C. L., Sakulyanontvittaya, T., Duhl, T., Emmons, L. K., and Wang, X.: The Model  
544 of Emissions of Gases and Aerosols from Nature version 2.1 (MEGAN2.1): an extended and updated framework  
545 for modeling biogenic emissions, *Geosci. Model Dev.*, 5, 1471-1492, 10.5194/gmd-5-1471-2012, 2012.

546 Han, Z., Xie, Z., Wang, G., Zhang, R., and Tao, J.: Modeling organic aerosols over east China using a volatility basis-  
547 set approach with aging mechanism in a regional air quality model, *Atmos. Environ.*, 124, Part B, 186-198,  
548 <http://dx.doi.org/10.1016/j.atmosenv.2015.05.045>, 2016.

549 Han, Z. W., Ueda, H., Matsuda, K., Zhang, R. J., Arao, K., Kanai, Y., and Hasome, H.: Model study on particle size  
550 segregation and deposition during Asian dust events in March 2002, *J. Geophys. Res.-Atmos.*, 109,  
551 10.1029/2004jd004920, 2004.

552 Harrison, R. M., and Yin, J. X.: Particulate matter in the atmosphere: which particle properties are important for its  
553 effects on health?, *Sci. Total Environ.*, 249, 85-101, 10.1016/s0048-9697(99)00513-6, 2000.

554 Heald, C. L., Jacob, D. J., Park, R. J., Russell, L. M., Huebert, B. J., Seinfeld, J. H., Liao, H., and Weber, R. J.: A  
555 large organic aerosol source in the free troposphere missing from current models, *Geophys. Res. Lett.*, 32,  
556 10.1029/2005gl023831, 2005.

557 Hu, J., Wang, P., Ying, Q., Zhang, H., Chen, J., Ge, X., Li, X., Jiang, J., Wang, S., Zhang, J., Zhao, Y., and Zhang,  
558 Y.: Modeling biogenic and anthropogenic secondary organic aerosol in China, *Atmos. Chem. Phys.*, 17, 77-92,  
559 10.5194/acp-17-77-2017, 2017.

560 Intergovernmental Panel on Climate Change (IPCC): *The Physical Science Basis of Climate Change: Changes in*  
561 *Atmospheric Constituents and in Radiative Forcing*, Cambridge University Press, New York, pp. 26-27, 2007.

562 Jacob, D. J.: Heterogeneous chemistry and tropospheric ozone, *Atmos. Environ.*, 34, 2131-2159, 10.1016/s1352-  
563 2310(99)00462-8, 2000.

564 Jiang, F., Liu, Q., Huang, X., Wang, T., Zhuang, B., and Xie, M.: Regional modeling of secondary organic aerosol  
565 over China using WRF/Chem, *J. Aerosol Sci.*, 43, 57-73, 10.1016/j.jaerosci.2011.09.003, 2012.

566 Jo, D. S., Park, R. J., Kim, M. J., and Spracklen, D. V.: Effects of chemical aging on global secondary organic aerosol  
567 using the volatility basis set approach, *Atmos. Environ.*, 81, 230-244, 10.1016/j.atmosenv.2013.08.055, 2013.

568 Juda-Rezler, K., Reizer, M., Huszar, P., Krueger, B. C., Zanis, P., Syrakov, D., Katragkou, E., Trapp, W., Melas, D.,  
569 Chervenkov, H., Tegoulas, I., and Halenka, T.: Modelling the effects of climate change on air quality over Central  
570 and Eastern Europe: concept, evaluation and projections, *Clim. Res.*, 53, 179-203, 10.3354/cr01072, 2012.

571 Kalberer, M., Paulsen, D., Sax, M., Steinbacher, M., Dommen, J., Prevot, A. S. H., Fisseha, R., Weingartner, E.,  
572 Frankevich, V., Zenobi, R., and Baltensperger, U.: Identification of polymers as major components of atmospheric  
573 organic aerosols, *Science*, 303, 1659-1662, 10.1126/science.1092185, 2004.

574 Kanakidou, M., Seinfeld, J. H., Pandis, S. N., Barnes, I., Dentener, F. J., Facchini, M. C., Van Dingenen, R., Ervens,  
575 B., Nenes, A., Nielsen, C. J., Swietlicki, E., Putaud, J. P., Balkanski, Y., Fuzzi, S., Horth, J., Moortgat, G. K.,  
576 Winterhalter, R., Myhre, C. E. L., Tsigaridis, K., Vignati, E., Stephanou, E. G., and Wilson, J.: Organic aerosol  
577 and global climate modelling: a review, *Atmos. Chem. Phys.*, 5, 1053-1123, 2005.

578 Kroll, J. H., Ng, N. L., Murphy, S. M., Flagan, R. C., and Seinfeld, J. H.: Secondary organic aerosol formation from  
579 isoprene photooxidation under high-NOx conditions, *Geophys. Res. Lett.*, 32, 10.1029/2005gl023637, 2005.

580 Kroll, J. H., Ng, N. L., Murphy, S. M., Flagan, R. C., and Seinfeld, J. H.: Secondary organic aerosol formation from  
581 isoprene photooxidation, *Environ. Sci. Technol.*, 40, 1869-1877, 10.1021/es0524301, 2006.

582 Kurokawa, J., Ohara, T., Morikawa, T., Hanayama, S., Janssens-Maenhout, G., Fukui, T., Kawashima, K., and  
583 Akimoto, H.: Emissions of air pollutants and greenhouse gases over Asian regions during 2000-2008: Regional  
584 Emission inventory in ASia (REAS) version 2, *Atmos. Chem. Phys.*, 13, 11019-11058, 10.5194/acp-13-11019-  
585 2013, 2013.

586 Lal, V., Khalizov, A. F., Lin, Y., Galvan, M. D., Connell, B. T., and Zhang, R.: Heterogeneous reactions of epoxides  
587 in acidic media, *J Phys Chem A*, 116, 6078-6090, 10.1021/jp2112704, 2012.

588 Lane, T. E., Donahue, N. M., and Pandis, S. N.: Simulating secondary organic aerosol formation using the volatility  
589 basis-set approach in a chemical transport model, *Atmos. Environ.*, 42, 7439-7451,  
590 10.1016/j.atmosenv.2008.06.026, 2008.

591 Li, J., Mao, J., Min, K.-E., Washenfelder, R. A., Brown, S. S., Kaiser, J., Keutsch, F. N., Volkamer, R., Wolfe, G. M.,  
592 Hanisco, T. F., Pollack, I. B., Ryerson, T. B., Graus, M., Gilman, J. B., Lerner, B. M., Warneke, C., de Gouw, J.  
593 A., Middlebrook, A. M., Liao, J., Welti, A., Henderson, B. H., McNeill, V. F., Hall, S. R., Ullmann, K., Donner, L.  
594 J., Paulot, F., and Horowitz, L. W.: Observational constraints on glyoxal production from isoprene oxidation and  
595 its contribution to organic aerosol over the Southeast United States, *J. Geophys. Res.-Atmos.*, 121, 9849-9861,  
596 10.1002/2016jd025331, 2016.

597 Li, J., Zhang, M., Wu, F., Sun, Y., and Tang, G.: Assessment of the impacts of aromatic VOC emissions and yields  
598 of SOA on SOA concentrations with the air quality model RAMS-CMAQ, *Atmos. Environ.*, 158, 105-115,  
599 10.1016/j.atmosenv.2017.03.035, 2017a.

600 Li, J., Zhang, M., Tang, G., Wu, F., Alvarado, L. M. A., Vrekoussis, M., Richter, A., and Burrows, J. P.: Investigating  
601 missing sources of glyoxal over China using a regional air quality model (RAMS-CMAQ), *Journal of*  
602 *Environmental Sciences*, 10.1016/j.jes.2018.04.021, 2018.

603 Li, L., Chen, C. H., Huang, C., Huang, H. Y., Zhang, G. F., Wang, Y. J., Wang, H. L., Lou, S. R., Qiao, L. P., Zhou,  
604 M., Chen, M. H., Chen, Y. R., Streets, D. G., Fu, J. S., and Jang, C. J.: Process analysis of regional ozone formation  
605 over the Yangtze River Delta, China using the Community Multi-scale Air Quality modeling system, *Atmos. Chem.*  
606 *Phys.*, 12, 10971-10987, 10.5194/acp-12-10971-2012, 2012.

607 Li, M., Zhang, Q., Kurokawa, J.-i., Woo, J.-H., He, K., Lu, Z., Ohara, T., Song, Y., Streets, D. G., Carmichael, G. R.,  
608 Cheng, Y., Hong, C., Huo, H., Jiang, X., Kang, S., Liu, F., Su, H., and Zheng, B.: MIX: a mosaic Asian  
609 anthropogenic emission inventory under the international collaboration framework of the MICS-Asia and HTAP,  
610 *Atmos. Chem. Phys.*, 17, 935-963, 10.5194/acp-17-935-2017, 2017b.

611 Li, N., Fu, T.-M., Cao, J., Lee, S., Huang, X.-F., He, L.-Y., Ho, K.-F., Fu, J. S., and Lam, Y.-F.: Sources of secondary  
612 organic aerosols in the Pearl River Delta region in fall: Contributions from the aqueous reactive uptake of  
613 dicarbonyls, *Atmos. Environ.*, 76, 200-207, 10.1016/j.atmosenv.2012.12.005, 2013.

614 Liggio, J., Li, S. M., and McLaren, R.: Reactive uptake of glyoxal by particulate matter, *Journal of Geophysical*  
615 *Research*, 110, 257-266, 2005.

616 Lim, Y. B., and Ziemann, P. J.: Products and mechanism of secondary organic aerosol formation from reactions of  
617 n-alkanes with OH radicals in the presence of NO<sub>x</sub>, *Environ. Sci. Technol.*, 39, 9229-9236, 10.1021/es051447g,  
618 2005.

619 Lim, Y. B., Tan, Y., Perri, M. J., Seitzinger, S. P., and Turpin, B. J.: Aqueous chemistry and its role in secondary  
620 organic aerosol (SOA) formation, *Atmos. Chem. Phys.*, 10, 10521-10539, 10.5194/acp-10-10521-2010, 2010.

621 Lin, G., Penner, J. E., Sillman, S., Taraborrelli, D., and Lelieveld, J.: Global modeling of SOA formation from  
622 dicarbonyls, epoxides, organic nitrates and peroxides, *Atmos. Chem. Phys.*, 12, 4743-4774, 10.5194/acp-12-4743-  
623 2012, 2012.

624 Lin, G., Sillman, S., Penner, J. E., and Ito, A.: Global modeling of SOA: the use of different mechanisms for aqueous-  
625 phase formation, *Atmos. Chem. Phys.*, 14, 5451-5475, 10.5194/acp-14-5451-2014, 2014.

626 Lin, J., An, J., Qu, Y., Chen, Y., Li, Y., Tang, Y., Wang, F., and Xiang, W.: Local and distant source contributions to  
627 secondary organic aerosol in the Beijing urban area in summer, *Atmos. Environ.*, 124, Part B, 176-185,  
628 <http://dx.doi.org/10.1016/j.atmosenv.2015.08.098>, 2016.

629 Lin, Y.-H., Zhang, H., Pye, H. O. T., Zhang, Z., Marth, W. J., Park, S., Arashiro, M., Cui, T., Budisulistiorini, H.,  
630 Sexton, K. G., Vizuete, W., Xie, Y., Luecken, D. J., Piletic, I. R., Edney, E. O., Bartolotti, L. J., Gold, A., and  
631 Surratt, J. D.: Epoxide as a precursor to secondary organic aerosol formation from isoprene photooxidation in the  
632 presence of nitrogen oxides, *Proceedings of the National Academy of Sciences of the United States of America*,  
633 110, 6718-6723, 10.1073/pnas.1221150110, 2013.

634 Liu, Z., Wang, Y., Vrekoussis, M., Richter, A., Wittrock, F., Burrows, J. P., Shao, M., Chang, C.-C., Liu, S.-C., Wang,  
635 H., and Chen, C.: Exploring the missing source of glyoxal (CHOCHO) over China, *Geophys. Res. Lett.*, 39,  
636 10.1029/2012gl051645, 2012.

637 Loeffler, K. W., Koehler, C. A., Paul, N. M., and De Haan, D. O.: Oligomer formation in evaporating aqueous glyoxal  
638 and methyl glyoxal solutions, *Environ. Sci. Technol.*, 40, 6318-6323, 10.1021/es060810w, 2006.

639 Morris, R. E., McNally, D. E., Tesche, T. W., Tonnesen, G., Boylan, J. W., and Brewer, P.: Preliminary evaluation of  
640 the community multiscale air, quality model for 2002 over the southeastern United States, *Journal of the Air &  
641 Waste Management Association*, 55, 1694-1708, 10.1080/10473289.2005.10464765, 2005.

642 Morris, R. E., Koo, B., Guenther, A., Yarwood, G., McNally, D., Tesche, T. W., Tonnesen, G., Boylan, J., and Brewer,  
643 P.: Model sensitivity evaluation for organic carbon using two multi-pollutant air quality models that simulate  
644 regional haze in the southeastern United States, *Atmos. Environ.*, 40, 4960-4972,  
645 10.1016/j.atmosenv.2005.09.088, 2006.

646 Murphy, B. N., and Pandis, S. N.: Simulating the Formation of Semivolatile Primary and Secondary Organic Aerosol  
647 in a Regional Chemical Transport Model, *Environ. Sci. Technol.*, 43, 4722-4728, 10.1021/es803168a, 2009.

648 Murphy, D. M., Cziczo, D. J., Froyd, K. D., Hudson, P. K., Matthew, B. M., Middlebrook, A. M., Peltier, R. E.,  
649 Sullivan, A., Thomson, D. S., and Weber, R. J.: Single-particle mass spectrometry of tropospheric aerosol particles,  
650 *J. Geophys. Res.: Atmos.*, 111, n/a-n/a, 10.1029/2006jd007340, 2006.

651 Myriokefalitakis, S., Vrekoussis, M., Tsigaridis, K., Wittrock, F., Richter, A., Bruehl, C., Volkamer, R., Burrows, J.  
652 P., and Kanakidou, M.: The influence of natural and anthropogenic secondary sources on the glyoxal global  
653 distribution, *Atmos. Chem. Phys.*, 8, 4965-4981, 2008.

654 Ng, N. L., Kroll, J. H., Chan, A. W. H., Chhabra, P. S., Flagan, R. C., and Seinfeld, J. H.: Secondary organic aerosol  
655 formation from m-xylene, toluene, and benzene, *Atmos. Chem. Phys.*, 7, 3909-3922, 2007.

656 Perry, R. H., and D. Green: *Perry's Chemical Engineers Handbook*, McGraw-Hill, New York, pp. 2-370, 1999.

657 Poschl, U.: *Atmospheric aerosols: Composition, transformation, climate and health effects*, *Angewandte Chemie-*  
658 *International Edition*, 44, 7520-7540, 10.1002/anie.200501122, 2005.

659 Randerson, J.T., van der Werf, G.R., Giglio, L., Collatz, G.J., Kasibhatla, P.S.: Global fire emissions database,  
660 version 4 (GFEDv4), Data set available on-line (<http://daac.ornl.gov/>) from Oak Ridge National Laboratory  
661 Distributed Active Archive Center, Oak Ridge, Tennessee, USA, [https://doi.org/10.3334/ ORNLDAAC/1293](https://doi.org/10.3334/ORNLDAAC/1293),  
662 2015.

663 Roberts, M. C., Andreae, M. O., Zhou, J. C., and Artaxo, P.: Cloud condensation nuclei in the Amazon Basin:  
664 "Marine" conditions over a continent?, *Geophys. Res. Lett.*, 28, 2807-2810, 2001.

665 Shrivastava, M. K., Lane, T. E., Donahue, N. M., Pandis, S. N., and Robinson, A. L.: Effects of gas particle  
666 partitioning and aging of primary emissions on urban and regional organic aerosol concentrations, *J. Geophys.*  
667 *Res.-Atmos.*, 113, 10.1029/2007jd009735, 2008.

668 Stavrakou, T., Mueller, J. F., De Smedt, I., Van Roozendaal, M., Kanakidou, M., Vrekoussis, M., Wittrock, F., Richter,  
669 A., and Burrows, J. P.: The continental source of glyoxal estimated by the synergistic use of spaceborne  
670 measurements and inverse modelling, *Atmos. Chem. Phys.*, 9, 8431-8446, 10.5194/acp-9-8431-2009, 2009.

671 Stavrakou, T., Peeters, J., and Muller, J. F.: Improved global modelling of HO<sub>x</sub> recycling in isoprene oxidation:  
672 evaluation against the GABRIEL and INTEX-A aircraft campaign measurements, *Atmos. Chem. Phys.*, 10, 9863-  
673 9878, 10.5194/acp-10-9863-2010, 2010.

674 Sun, J., Wu, F., Hu, B., Tang, G., Zhang, J., and Wang, Y.: VOC characteristics, emissions and contributions to SOA  
675 formation during hazy episodes, *Atmos. Environ.*, 141, 560-570, 10.1016/j.atmosenv.2016.06.060, 2016.

676 Surratt, J. D., Lewandowski, M., Offenberg, J. H., Jaoui, M., Kleindienst, T. E., Edney, E. O., and Seinfeld, J. H.:  
677 Effect of acidity on secondary organic aerosol formation from isoprene, *Environ. Sci. Technol.*, 41, 5363-5369,  
678 10.1021/es0704176, 2007.

679 Tsigaridis, K., Daskalakis, N., Kanakidou, M., Adams, P. J., Artaxo, P., Bahadur, R., Balkanski, Y., Bauer, S. E.,  
680 Bellouin, N., Benedetti, A., Bergman, T., Berntsen, T. K., Beukes, J. P., Bian, H., Carslaw, K. S., Chin, M., Curci,  
681 G., Diehl, T., Easter, R. C., Ghan, S. J., Gong, S. L., Hodzic, A., Hoyle, C. R., Iversen, T., Jathar, S., Jimenez, J.  
682 L., Kaiser, J. W., Kirkevåg, A., Koch, D., Kokkola, H., Lee, Y. H., Lin, G., Liu, X., Luo, G., Ma, X., Mann, G. W.,  
683 Mihalopoulos, N., Morcrette, J. J., Mueller, J. F., Myhre, G., Myriokefalitakis, S., Ng, N. L., O'Donnell, D., Penner,  
684 J. E., Pozzoli, L., Pringle, K. J., Russell, L. M., Schulz, M., Sciare, J., Seland, O., Shindell, D. T., Sillman, S.,  
685 Skeie, R. B., Spracklen, D., Stavrakou, T., Steenrod, S. D., Takemura, T., Tiitta, P., Tilmes, S., Tost, H., van Noije,  
686 T., van Zyl, P. G., von Salzen, K., Yu, F., Wang, Z., Wang, Z., Zaveri, R. A., Zhang, H., Zhang, K., Zhang, Q., and  
687 Zhang, X.: The AeroCom evaluation and intercomparison of organic aerosol in global models, *Atmos. Chem.*  
688 *Phys.*, 14, 10845-10895, 10.5194/acp-14-10845-2014, 2014.

689 Volkamer, R., Jimenez, J. L., San Martini, F., Dzepina, K., Zhang, Q., Salcedo, D., Molina, L. T., Worsnop, D. R.,  
690 and Molina, M. J.: Secondary organic aerosol formation from anthropogenic air pollution: Rapid and higher than  
691 expected, *Geophys. Res. Lett.*, 33, 10.1029/2006gl026899, 2006.

692 Wang, F., An, J., Li, Y., Tang, Y., Lin, J., Qu, Y., Chen, Y., Zhang, B., and Zhai, J.: Impacts of uncertainty in AVOC  
693 emissions on the summer RO<sub>x</sub> budget and ozone production rate in the three most rapidly-developing economic  
694 growth regions of China, *Advances in Atmospheric Sciences*, 31, 1331-1342, 10.1007/s00376-014-3251-z, 2014.

695 Warneck, P.: In-cloud chemistry opens pathway to the formation of oxalic acid in the marine atmosphere, *Atmos.*  
696 *Environ.*, 37, 2423-2427, 10.1016/s1352-2310(03)00136-5, 2003.

697 Willmott, C. J.: ON THE VALIDATION OF MODELS, *Physical Geography*, 2, 184-194,  
698 10.1080/02723646.1981.10642213, 1981.

699 Woo, J. L., and McNeill, V. F.: simpleGAMMA v1.0-a reduced model of secondary organic aerosol formation in the  
700 aqueous aerosol phase (aaSOA), *Geosci. Model Dev.*, 8, 1821-1829, 10.5194/gmd-8-1821-2015, 2015.

701 Wu, F., Yu, Y., Sun, J., Zhang, J., Wang, J., Tang, G., and Wang, Y.: Characteristics, source apportionment and  
702 reactivity of ambient volatile organic compounds at Dinghu Mountain in Guangdong Province, China, *Sci. Total*  
703 *Environ.*, 548, 347-359, <http://dx.doi.org/10.1016/j.scitotenv.2015.11.069>, 2016.

704 Xu, W., Han, T., Du, W., Wang, Q., Chen, C., Zhao, J., Zhang, Y., Li, J., Fu, P., Wang, Z., Worsnop, D. R., and Sun,  
705 Y.: Effects of Aqueous-Phase and Photochemical Processing on Secondary Organic Aerosol Formation and  
706 Evolution in Beijing, China, *Environ. Sci. Technol.*, 51, 762-770, 10.1021/acs.est.6b04498, 2017.

707 Xu, W. Q., Sun, Y. L., Chen, C., Du, W., Han, T. T., Wang, Q. Q., Fu, P. Q., Wang, Z. F., Zhao, X. J., Zhou, L. B., Ji,  
708 D. S., Wang, P. C., and Worsnop, D. R.: Aerosol composition, oxidation properties, and sources in Beijing: results  
709 from the 2014 Asia-Pacific Economic Cooperation summit study, *Atmos. Chem. Phys.*, 15, 13681-13698,  
710 10.5194/acp-15-13681-2015, 2015.

711 Ying, Q., Li, J., and Kota, S. H.: Significant Contributions of Isoprene to Summertime Secondary Organic Aerosol

712 in Eastern United States, *Environ. Sci. Technol.*, 49, 7834-7842, 10.1021/acs.est.5b02514, 2015.

713 Yu, S., Mathur, R., Schere, K., Kang, D., Pleim, J., Young, J., Tong, D., Pouliot, G., McKeen, S. A., and Rao, S. T.:

714 Evaluation of real-time PM<sub>2.5</sub> forecasts and process analysis for PM<sub>2.5</sub> formation over the eastern United States

715 using the Eta-CMAQ forecast model during the 2004 ICARTT study, *J. Geophys. Res.-Atmos.*, 113,

716 10.1029/2007jd009226, 2008.

717 Zhang, H., and Ying, Q.: Secondary organic aerosol formation and source apportionment in Southeast Texas, *Atmos.*

718 *Environ.*, 45, 3217-3227, 10.1016/j.atmosenv.2011.03.046, 2011.

719 Zhang, H., Li, J., Ying, Q., Yu, J. Z., Wu, D., Cheng, Y., He, K., and Jiang, J.: Source apportionment of PM<sub>2.5</sub> nitrate

720 and sulfate in China using a source-oriented chemical transport model, *Atmos. Environ.*, 62, 228-242,

721 <https://doi.org/10.1016/j.atmosenv.2012.08.014>, 2012.

722 Zhang, H., and Ying, Q.: Secondary organic aerosol from polycyclic aromatic hydrocarbons in Southeast Texas,

723 *Atmos. Environ.*, 55, 279-287, 10.1016/j.atmosenv.2012.03.043, 2012.

724 Zhang, Q., Jimenez, J. L., Canagaratna, M. R., Allan, J. D., Coe, H., Ulbrich, I., Alfarra, M. R., Takami, A.,

725 Middlebrook, A. M., Sun, Y. L., Dzepina, K., Dunlea, E., Docherty, K., DeCarlo, P. F., Salcedo, D., Onasch, T.,

726 Jayne, J. T., Miyoshi, T., Shimojo, A., Hatakeyama, S., Takegawa, N., Kondo, Y., Schneider, J., Drewnick, F.,

727 Borrmann, S., Weimer, S., Demerjian, K., Williams, P., Bower, K., Bahreini, R., Cottrell, L., Griffin, R. J.,

728 Rautiainen, J., Sun, J. Y., Zhang, Y. M., and Worsnop, D. R.: Ubiquity and dominance of oxygenated species in

729 organic aerosols in anthropogenically-influenced Northern Hemisphere midlatitudes, *Geophys. Res. Lett.*, 34,

730 10.1029/2007gl029979, 2007.

731

732

733

734

735

736

737

738

739

740

741

742

743

744

745

746

747

748

749

750

751

752

753

754

755

756 Table 1. Statistics for the meteorological variables and PM<sub>2.5</sub> between the simulated and observed data during the  
 757 two episodes.

Table 1-1

Variables	Episode	<i>N</i>	<i>C<sub>mod</sub></i>	<i>C<sub>obs</sub></i>	MB	RMSE	<i>R</i>	IOA
Temperature (°C)	1	10770	23.76	24.59	-0.83	2.58	0.86	0.91
	2	8391	12.68	13.36	-0.68	3.13	0.92	0.95
Relative humidity (%)	1	10770	69.42	67.90	1.52	13.68	0.83	0.91
	2	8389	62.81	62.86	-0.05	14.73	0.77	0.88
Wind speed (m/s)	1	10770	1.78	2.18	-0.40	1.64	0.35	0.61
	2	8391	2.05	2.27	-0.22	1.75	0.50	0.69

Table 1-2

Variables	Episode	<i>N</i>	<i>C<sub>mod</sub></i>	<i>C<sub>obs</sub></i>	FB (%)	FE (%)	<i>R</i>	IOA
PM <sub>2.5</sub> (µg/m <sup>3</sup> )	1	8091	64.04	47.90	13.35	64.61	0.50	0.64
	2	7649	86.25	61.67	36.00	62.27	0.56	0.70

Table 1-3

Variables	Episode	<i>N</i>	P <sub>22.5°</sub> (%)	P <sub>45°</sub> (%)
Wind direction (°)	1	10770	32.12	54.52
	2	8391	34.01	57.41

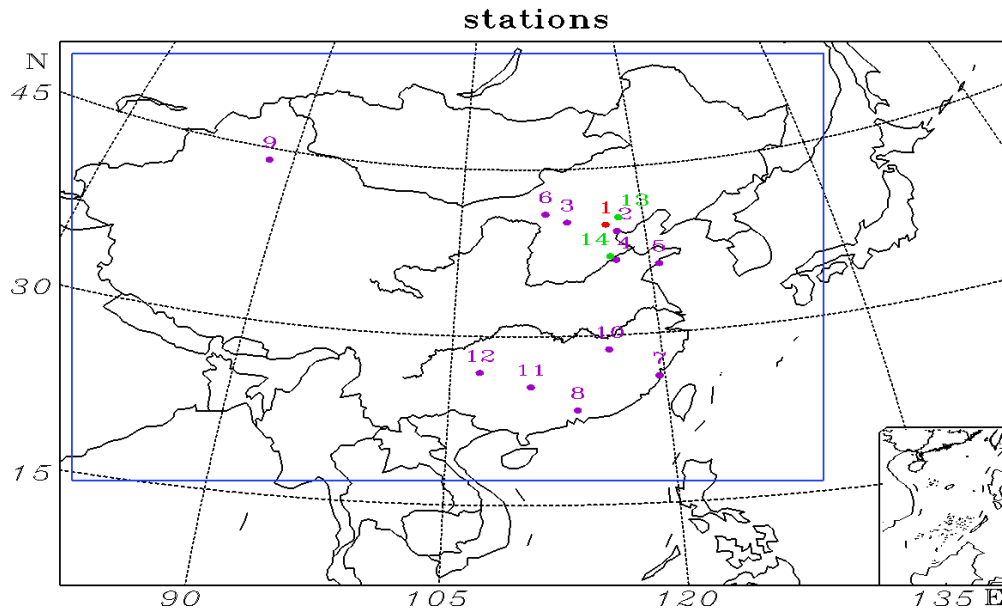
758 *N* is the total number of samples; *C<sub>mod</sub>* and *C<sub>obs</sub>* are the average value of modeled and observed results, respectively;  
 759 MB and FB are the mean and fractional bias, respectively; RMSE and FE are the root-mean-square and fractional  
 760 error, respectively; IOA is the index of agreement; *R* is the correlation coefficient between the observed and simulated  
 761 results; P<sub>22.5°</sub> and P<sub>45°</sub> represent the proportions of compared results that the absolute biases between the simulated  
 762 and measured wind directions are within 22.5° and 45°, respectively.

763

764 Table 2. Performance statistics of the modeled and observed SOA concentrations (µg/m<sup>3</sup>).

Case	Episode	<i>N</i>	<i>C<sub>model</sub></i>	<i>C<sub>obs</sub></i>	MB	RMSE	<i>R</i>	IOA
0	1	822	2.21	12.69	-10.48	13.48	0.21	0.46
	2	737	1.05	17.69	-16.64	23.52	0.83	0.45
1	1	822	5.86	12.69	-6.83	10.86	0.25	0.49
	2	737	2.87	17.69	-14.82	21.21	0.84	0.50
2	1	822	12.03	12.69	-0.66	10.19	0.21	0.52
	2	737	6.53	17.69	-11.16	16.56	0.83	0.64

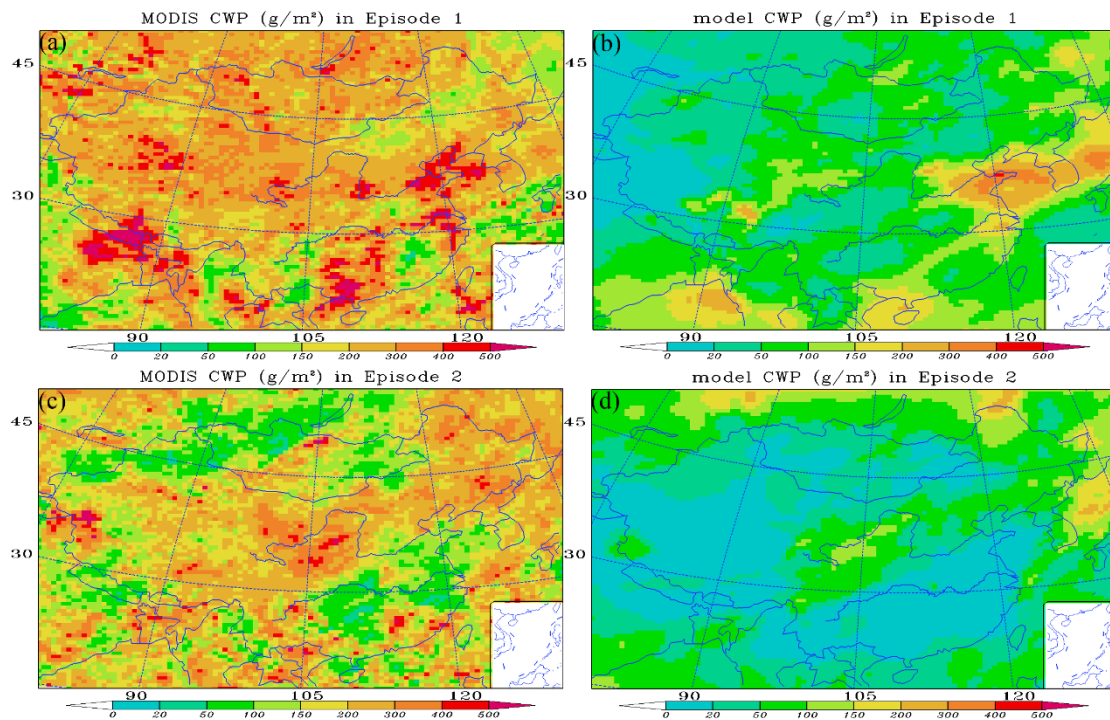
765



766

767 Fig. 1. Geographical locations of the measurement stations in the model domain. 1: Beijing; 2: Tianjin; 3: Datong;  
 768 4: Jinan; 5: Qingdao; 6: Hohhot; 7: Fuzhou; 8: Guangzhou; 9: Urumqi; 10: Nanchang; 11: Guilin; 12: Guiyang; 13:  
 769 Xinglong; 14: Yucheng. The different colors denote which variables are compared at each station: purple:  
 770 meteorological parameters; green: concentrations of aromatics; red: both meteorological parameters and aromatic  
 771 compound concentrations.

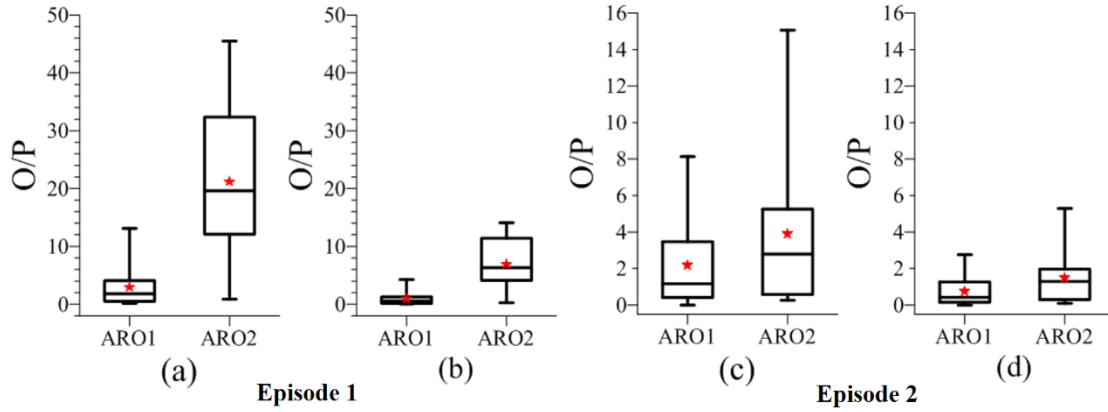
772



773

774 Fig. 2. Observed and simulated distributions of the mean cloud water path (CWP) during the two episodes (left-hand  
 775 panels: MODIS observation; right-hand panels: results of simulations).

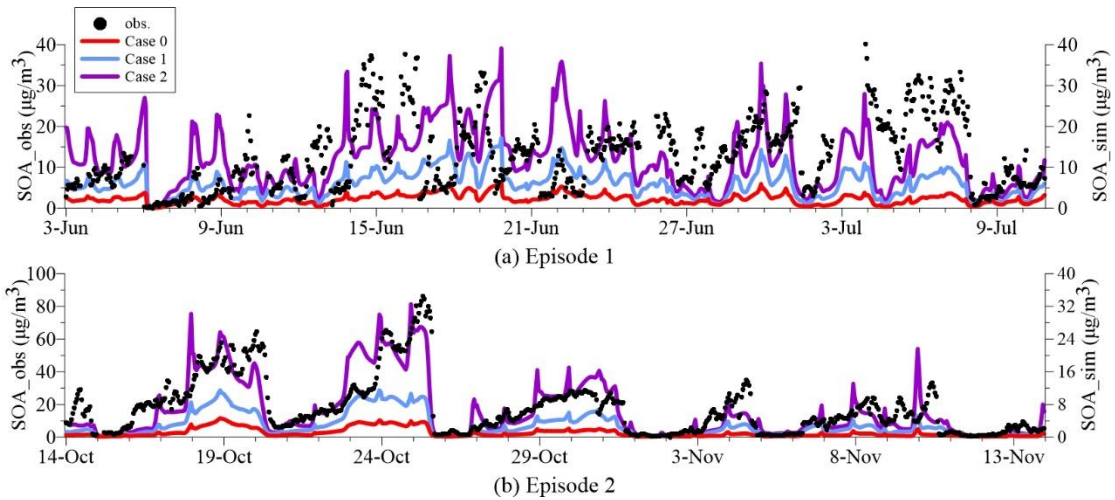




776

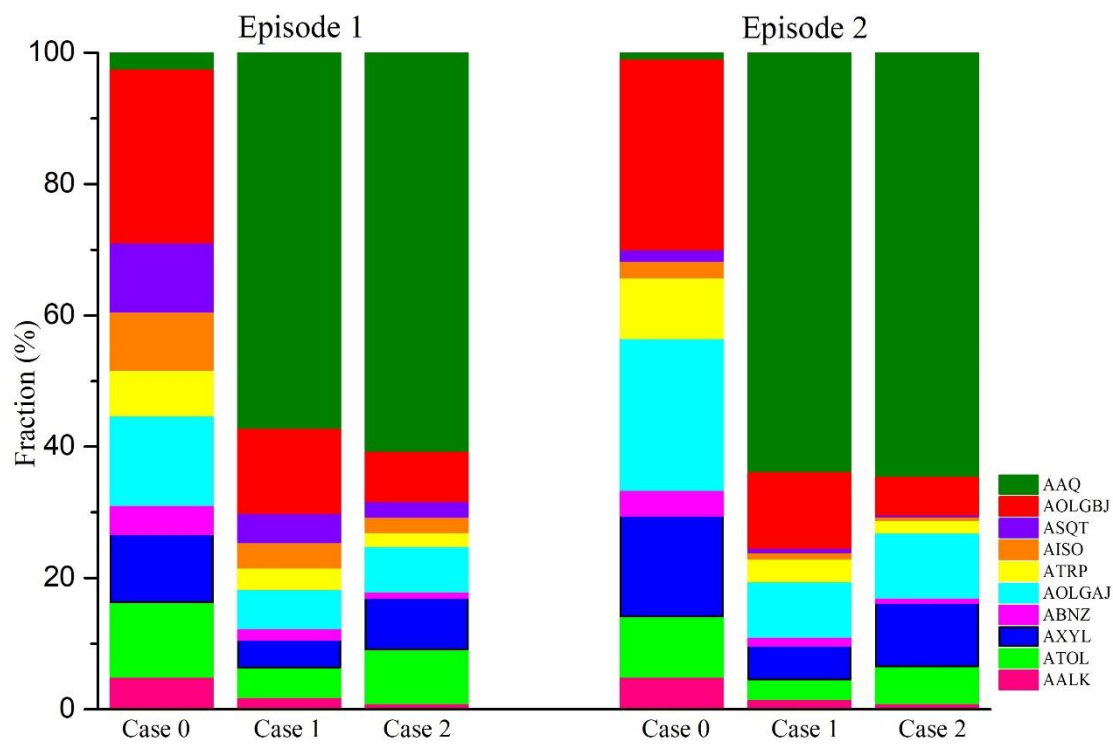
777 Fig. 3. Box-whisker plot of the observed to predicted (O/P) ratios of aromatic compounds during the two analyzed  
 778 episodes. The observed data were measured at 14:00 LST every Thursday by gas chromatography-mass spectrometer  
 779 at three sites (Beijing, Xinglong and Yucheng). (a, c): Original emissions of aromatic compounds; and (b, d): a three-  
 780 fold increase in the emissions of aromatic compounds. The red stars show the mean O/P ratios.

781



782

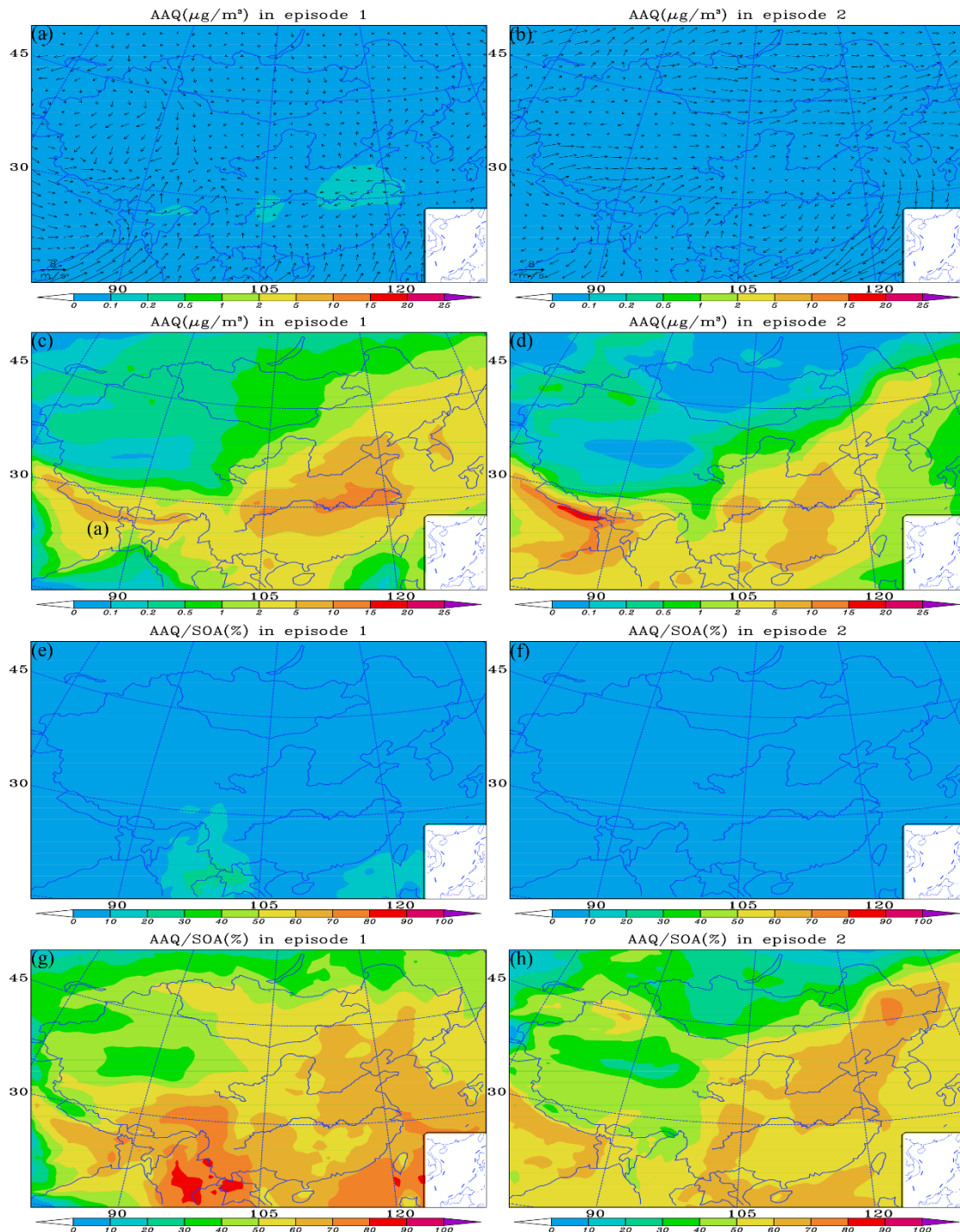
783 Fig. 4. Hourly concentrations of the observed and simulated near-surface SOA concentrations in episode 1 (a) and 2  
 784 (b). Case 0 is base run; case 1 is run with the incorporation of the reactive uptake of dicarbonyls (excluding the  
 785 default in-cloud dicarbonyl oxidations); and case 2 is run with the glyoxal underestimation taken into consideration  
 786 based on case 1.



787

788 Fig. 5. Mean contributions from different sources of SOAs in the three sensitivity case studies during the two  
 789 analyzed episodes. The compositions represent the SOA formed from long-chain alkanes (AALK), high-yield  
 790 aromatic compounds (ATOL), low-yield aromatic compounds (AXYL), benzene (ABNZ), monoterpenes (ATRP),  
 791 isoprene (AISO), sesquiterpenes (ASQT) and dicarbonyls (AAQ), as well as aged anthropogenic (AOLGAJ) and  
 792 biogenic SOA (AOLGBJ). Case 0 is the base run; case 1 is run with the incorporation of the reactive uptake of  
 793 dicarbonyls (excluding the default in-cloud dicarbonyl oxidations); and case 2 is based on case 1, but taking into  
 794 consideration the underestimation of glyoxal

795



796

797 Fig. 6. Modeled distributions of the mean (a, b) wind field with SOA formed from dicarbonyls (AAQ) in case 0, (c,  
 798 d) AAQ in case 2, (e, f) AAQ/SOA in case 0, (g, h) AAQ/SOA in case 2, over the regions during two episodes. Case  
 799 0 is the base run; case 2 is run taking into consideration the incorporation of the reactive uptake of dicarbonyls  
 800 (excluding the default in-cloud dicarbonyl oxidations) and the underestimation of glyoxal.